J Comp Physiol A (1996) 178: 359–371

ORIGINAL PAPER

S. Coombs · M. Hastings · J. Finneran

Modeling and measuring lateral line excitation patterns to changing dipole source locations

Accepted: 24 August 1995

Abstract In order to determine excitation patterns to the lateral line system from a nearby 50 Hz oscillating sphere, dipole flow field equations were used to model the spatial distribution of pressures along a linear array of lateral line canal pores. Modeled predictions were then compared to pressure distributions measured for the same dipole source with a miniature hydrophone placed in a small test tank used for neurophysiological experiments. Finally, neural responses from posterior lateral line nerve fibers in the goldfish were measured in the test tank to demonstrate that modeled and measured pressure gradient patterns were encoded by the lateral line periphery. Response patterns to a 50 Hz dipole source that slowly changed location along the length of the fish included (1) peaks and valleys in spike-rate responses corresponding to changes in pressure gradient amplitudes, (2) 180° phase-shifts corresponding to reversals in the direction of the pressure gradient and (3) distance-dependent changes in the locations of peaks, valleys and 180° phase-shifts. Modeled pressure gradient patterns also predict that the number of neural amplitude peaks and phase transitions will vary as a function of neuromast orientation and axis of source oscillation. The faithful way in which the lateral line periphery encodes pressure gradient patterns has implications for how source location and distance might be encoded by excitation patterns in the CNS. Phase-shift information may be important for (1) inhibitory/excitatory sculpting of receptive fields and (2) unambiguously encoding source distance so that increases in source distance are not confused with decreases in source amplitude.

S. Coombs (✉)
Parmly Hearing Institute, Loyola University of Chicago, Chicago Il 60626, USA

M. Hastings · J. Finneran
Department of Mechanical Engineering, Ohio State University, Columbus, OH 43210, USA

Key words Lateral line · Distance determination · Receptive fields · Excitation patterns · Source localization

Introduction

The mechanisms by which sound source location is encoded by the nervous system of aquatic vertebrates is poorly understood relative to those used by terrestrial vertebrates. This is primarily because the cues available for localizing air-borne sounds, such as binaural time and intensity differences, are minimized in aquatic environments due to the greater speed of sound in water and the lack of significant density differences between the animal and the surrounding water (van Bergeijk 1964). In the nearfield of a dipole sound source, however, spatial non-uniformities in the pressure field (Denton and Gray 1983, 1993; Kalmijn 1988, 1989) are also available as potential cues that can be detected by the lateral line system of fish. In fact, excitation of the lateral line system depends on these non-uniformities (Kalmijn 1988, 1989). These cues are also thought to be more useful for aquatic vertebrates, since for any given sound frequency, the extent of the nearfield in water is roughly five times that in air. At a frequency of 50 Hz, for example, the nearfield extends to about 10 meters in water relative to 2 m in air.

In a series of studies on the mechanics of lateral line stimulation (Denton and Gray 1983; Gray 1984; Gray and Best 1989), Gray and colleagues provided some of the first evidence that source location could be encoded by the pattern of excitation that occurs among the spatially-distributed endorgans (neuromasts) of the lateral line system. On the basis of calculated stimulus levels at different canal neuromasts along the head and trunk of the ruffe, *Gymnocephalus cernua*, Gray and Best (1989) predicted that there would be rather large changes in both the level and phase of neural responses across neuromasts in a given canal corresponding to

changes as small as 5 mm in the position of the fish relative to a small (1.5 mm in diameter) dipole source. More recently, Hassan (1993) has described the spatial distribution of dipole flow fields in three dimensions, taking into account source location and orientation, and the hydrodynamic interaction between the fish and the flow field.

Whereas these earlier studies provide theoretical information on spatial non-uniformites and flow field patterns that might be used in source localization, there still remains very little information on how or if these patterns are encoded by the peripheral and central nervous system. Furthermore, the earlier theoretical work is not easily translated into an experimental situation in which neural response patterns can be directly related to stimulus patterns.

In this paper, we present a new approach that (1) combines elements of previous theoretical approaches for predicting the spatial distribution of the stimulus field and (2) adapts a stimulus presentation and data analysis approach used by Bastian (1981a, b) for measuring neural responses from electroreceptive fish. Stimulus presentation is accomplished with a dipole source that slowly, but continuously changes location along the length of the fish. Neurophysiological techniques are used to record the responses of peripheral lateral line fibers to the changing locations of the dipole source. Changes in the response are compared with pressure gradient changes that have been measured and mathematically modeled for the same source characteristics and locations used in neurophysiological studies. The purpose of this paper is to (1) describe the basic methodological approach and its assumptions, (2) to systematically describe the pressure gradient patterns generated by the moving dipole source for different distances and axes of oscillation, (3) to demonstrate that the pressure gradient patterns are represented in the neural responses of peripheral lateral line nerve fibers and (4) to present new neurophysiological and modeling results on how source distance might be encoded by the lateral line system.

Methods

Computer modeling

Excitation patterns for the lateral line trunk canal were modeled as pressure gradient patterns, calculated from the flow field equations for a dipole source (Morse 1948; Kalmijn 1988). The use of pressure gradient patterns to predict excitation patterns was based on the following assumptions: (1) there is a single neuromast between every two pores on the trunk canal and (2) the response of each neuromast to fluid motions inside the canal is proportional to the outside pressure gradient (which, in turn, is proportional to the particle acceleration of the water) across the two pores. The latter assumption differs somewhat from that used by Denton and Gray (1983) in that we are modeling the acceleration of the surrounding water and not the net acceleration between the fish and surrounding water. We do so because the fish is rigidly held under the conditions of neurophysiological experiments. Thus, we assume the acceleration of the fish to be negligible.

MATLAB (Version 4.0, The Mathworks, Inc.) was used to program the flow field equations for a dipole source of the same size and stimulus dimensions of that used in neurophysiological experiments (see STIMULUS GENERATION). Pressure amplitude (P) was calculated as $P = [(\rho\omega a^3 U)/2r^2]\cos\theta$, where ρ = ambient density, $\omega = 2\pi f$, r = distance from source center, $\theta = 0°$ along the axis of oscillation, and a = source (sphere) radius. Source oscillation amplitude (U) was arbitrarily defined as 1 m/s, where $U = 2\pi fd$ and d = maximum displacement of the source. All modeling was based on the properties of fresh water at standard temperature and atmospheric pressure.

In order to predict lateral line excitation patterns, the lateral line trunk canal of the goldfish was modeled as a simple tube with a series of pressure sampling points (pores) as illustrated in Fig. 1A. Pressure sampling points were separated by 2 mm intervals, the

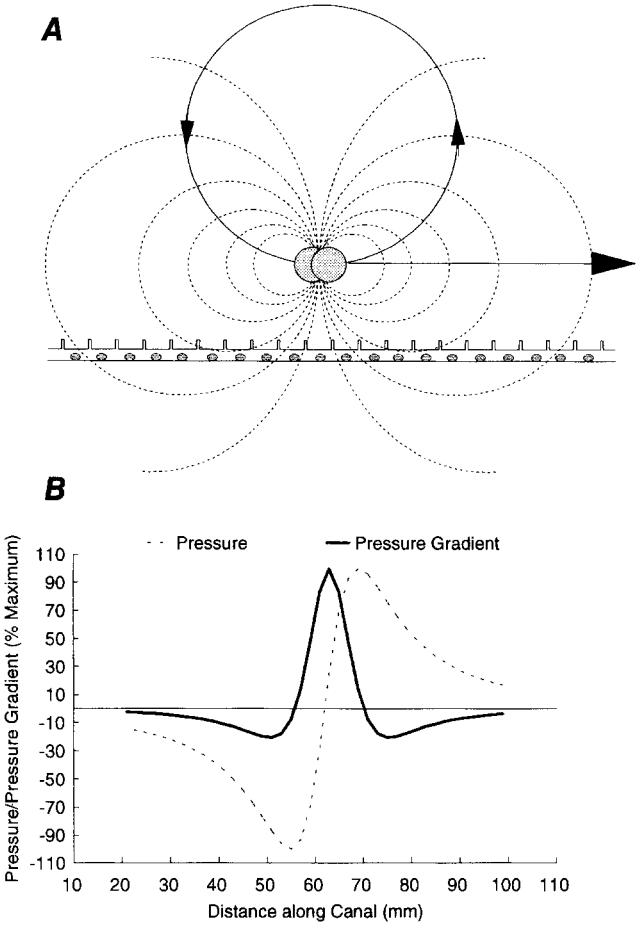

Fig. 1 **A** Schematic representation of iso-pressure contours (*dashed lines*) and flow lines (*solid lines with arrows*) about a dipole source. Iso-pressure contours are depicted for a single plane that bisects the source along its axis of oscillation, indicated by the large arrow head to the right of the source. The lateral line trunk canal of the goldfish is modeled as a simple tube with an array of pressure sampling points (canal pores) separated by 2 mm intervals (not to scale). In this example, the modeled canal is confined to a single horizontal plane through source center and it's long axis is parallel to the axis of source oscillation. **B** Corresponding plots of pressure (*dashed line*) and pressure gradient (*solid line*) distributions across the modeled trunk canal. Note that the maximum pressure gradient is centered at the source, arbitrarily located at x distance = 61 mm along the modeled canal

average interpore distance on the trunk canal of the goldfish. In the example shown in Fig. 1, the tube is parallel to the axis of source oscillation, 10 mm away from the center of the source and confined to a single horizontal plane through the source center. We used the MATLAB software to compute the pressure amplitudes at each pore (dashed line in Fig. 1B) and the pressure differences (solid line, Fig. 1B) between each successive pair of pores. The distance and orientation of the tube with respect to the source was then varied to predict how pressure gradient patterns would change.

Stimulus generation

The dipole sound source used in neurophysiological experiments and stimulus measurements consisted of a small (6 mm in diameter), sinusoidally-oscillating (50 Hz) plastic sphere rigidly-attached to a minishaker (B & K 4810) by a stainless steel, blunt-tipped needle (16 guage, 12 mm in length). The shaft (needle) was mounted perpendicular to the shaker diaphragm to produce sinusoidal oscillations in the horizontal plane along a rostral-caudal axis relative to the fish or hydrophone. The amplitude and frequency of oscillation were computer controlled through a Tucker-Davis D/A module. Sinusoidal oscillation and linear motion were gated on and off simultaneously; rise/fall times of sinusoidal signals were 10 ms and sinusoids were gated on at 0° starting phases.

For both neurophysiological experiments and stimulus measurement, the location of the dipole source was continuously changed at the rate of 4 mm/s along a single linear axis (X-axis of Fig. 1) spanning between 50–80 mm. This was accomplished by mounting the minishaker to a sliding plate, moved by a worm-gear assembly (Velmex, Inc.) that was driven by a stepper motor under computer control. This assembly was in turn mounted to independently-controlled X, Y and Z assemblies that enabled precise positioning of the source (relative to the fish or hydrophone) in all 3 dimensions before continuous movement of the source along the X-axis (along the fish's body) was begun.

Stimulus measurement

The sound pressure associated with the changing locations of the dipole source was measured with a miniature hydrophone (B & K 8103) positioned at the middle of the X-axis range of linear motion and at varying distances (Y axis) and elevations (Z axis) with respect to the axis of source motion (Fig. 2). Measurements were made in the physiological test tank at the same location of the fish, but in the absence of the fish. All other stimulus conditions were maintained identical to that used in physiological experiments. The time-waveform of the hydrophone output was digitized (Tucker-Davis A/D module) and used to compute the average RMS amplitude over each 2 mm segment of linear motion. Amplitude spectra and instantaneous frequency were also obtained from a fast fourier transform of the digitized waveform.

Neural response measurement and analysis

Methods for recording evoked activity from single fibers of the posterior lateral line nerve in the goldfish were very similar to those used previously on the mottled sculpin (Coombs and Janssen 1990). Goldfish, ranging from 9–12 cm in standard length, were obtained from commercial outlets and housed in 20 gal aquaria. Protocols for the handling of animals have been approved by and are on file with Loyola's Institutional Animal Care and Use Committee.

Fish were anesthetized by immersion in MS-222 (0.01%) and immobilized with intramuscular injections of Flaxedil (0.1 mg/gm body weight). Fish were then transferred to the experimental tank (16.5 × 17.8 × 36.8 cm) and their heads clamped onto a respirator

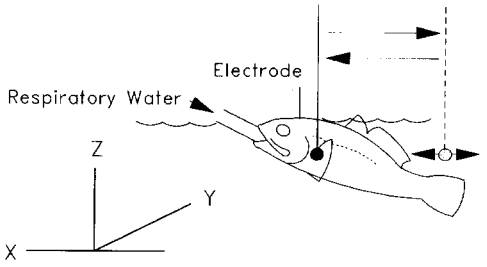

Fig. 2 Schematic diagram of source motion (*X-axis*) and 3-dimensional positioning of the source relative to the fish in neurophysiological set-up. Stimulus motion and positioning was the same for hydrophone measurements of pressure fields, except that the hydrophone replaced the fish

tube that fed water through the mouth and over the gills. The dorsal portion of the cranium was positioned above water, but the trunk of the fish was submerged at a slight (10–20°) angle from the horizontal plane (Fig. 2). The overflow drain in the front of the tank kept respiratory flows localized near the head end of the animal and flow levels were kept below those that produced discernable effects on posterior lateral line nerve fibers.

Once the animal was positioned in the tank, a hole was made in the top of the skull to expose the brain, and excess fatty tissue and fluids were aspirated away to reveal the posterior lateral line nerve root where it entered the brainstem. Two-percent lidocaine was injected intramuscularly at 2-h intervals near the surgical wound. Micropipettes filled with 3 *M* KCl (tip impedance ranging from 10 to 50 MΩ) were placed on the nerve with a micromanipulator and advanced through the nerve with a motorized microdrive. The output of the microelectrode was amplified within a 300 to 3000 Hz bandwidth, and single spikes were distinguished by a voltage-level discriminator that converted them into TTL pulses. Data acquisition components of a modular hardware system (Tucker Davis) recorded TTL pulses in the form of elapsed times from stimulus onset to the occurence of the TTL pulse.

Evoked activity was recorded in response to a dipole source (see STIMULUS GENERATION) that slowly changed its position in a head-tail and then a tail-head direction (Fig. 2) for 5 repetitions in each direction. The axis of oscillation was kept parallel to the axis of motion for all response measurements. As the source moved, its relative position along the length of the fish (X-position) changed, whereas its distance (Y-position) from the fish's lateral body surface and it's elevation (Z-position) remained relatively constant. Since the X-axis of motion had to be kept perfectly horizontal to assure smooth operation of the worm gear, the axis of dipole motion and oscillation deviated slightly from the long axis of the fish (Fig. 2).

Neural responses to the changing locations were summarized in a spatial event plot (SEP) that relates the change in responsiveness to the X-position of the source. To ensure that neural response patterns were governed primarily by source location and not by other factors, such as the slow linear motion, we also ran three control conditions: sinusoidal oscillation of the sphere in the absence of linear motion, linear motion in the absence of oscillation and the absence of both oscillation and linear motion.

Neural responsiveness was measured for each 2 mm segment of motion (= 500 ms or 25 sinusoidal cycles) to yield location-specific measurements of (1) the average firing rate (spikes/s), (2) the average phase angle (degrees) of spike times with respect to the signal to the minishaker and (3) the Raleigh statistic, Z. Both the phase angle and Z were determined by collapsing elapsed spike times into a single period histogram and determining the phase angle and length of the mean histogram vector, R. $Z = R^{2*}N$, where N = total number of spikes (Batschelet 1981). Response values at each location were then averaged over 5 repetitions of movement for each direction.

The Raleigh statistic was used in two ways: (1) as a combined measure of firing rate and phase-locking to the sinuosidal stimulus

and (2) as a statistical test of whether or not phase-locking and phase angle measures were drawn from a randomly distributed sample population (e.g. the period histogram). Z values above about 4.6 indicate a probality of less than 0.01 that the period histogram distribution was random (Table 4.2.1 from Batschelet 1981).

Results

Stimulus measurement and matlab modeling

Plotted in Fig. 1B are the computer predictions for pressure levels (dashed line) at each of the modeled canal pores and for the pressure gradient (solid line) across each consecutive pair of pores. Pressures to the right of the source are arbitrarily plotted as positive and those to the left as negative to depict 180° phase differences. Figure 3 shows the digitized waveform of the pressure-sensitive hydrophone's response to a 50 Hz oscillating sphere as it moves past the hydrophone. The axis of sinusoidal oscillation is along the X-axis of linear motion; the source is 10 mm away from and at the same elevation as the acoustic center of the hydrophone. Starting with trace 1 at the bottom of this figure, each trace represents successive 1000 ms (= 4 mm of travel) segments of the hydrophone's response to the moving source. The hydrophone response shows that as the sphere gets closer to the hydrophone, the P-P pressure amplitude (dashed line of Fig. 1B) rises until just before the source reaches the hydrophone. When the source is about 1 cm away from the hydrophone, the P-P pressure starts to decline, falling near zero when the source is directly opposite the hydrophone (see middle of trace 11). As the source moves past the hydrophone, the response increases again to form a mirror-image of the time waveform that preceded it. A time-compressed version of this same waveform is shown in Fig. 4 (top panel) along with its amplitude spectrum (middle panel) and instantaneous frequency (bottom panel). The null in the center of the time waveform relates to the fact that the pressure field about a dipole source is bilaterally symmetrical, radiating in two directions with a pressure null centered at the source (Fig. 1). Coincident with the null is an abrupt 180° phase reversal in the response (compare phase of

Fig. 3 Digitized time-waveform of hydrophone response to a 50 Hz oscillating sphere as it moves past the hydrophone. Starting with trace 1 at the bottom (from left to right), each trace represents successive 1000 ms (= 4 mm) segments of the hydrophone's response to the dipolar source. Note that after the response null in the middle of trace 11, there is a 180° change in the phase response. The axis of sinusoidal oscillation is along the axis of linear motion. For an X-position of 0 (source directly opposite the hydrophone), the Y-position of the source is 10 mm away from the acoustic center of the hydrophone and the Z-position is 0 mm (i.e. at the same elevation as the acoustic center of the hydrophone)

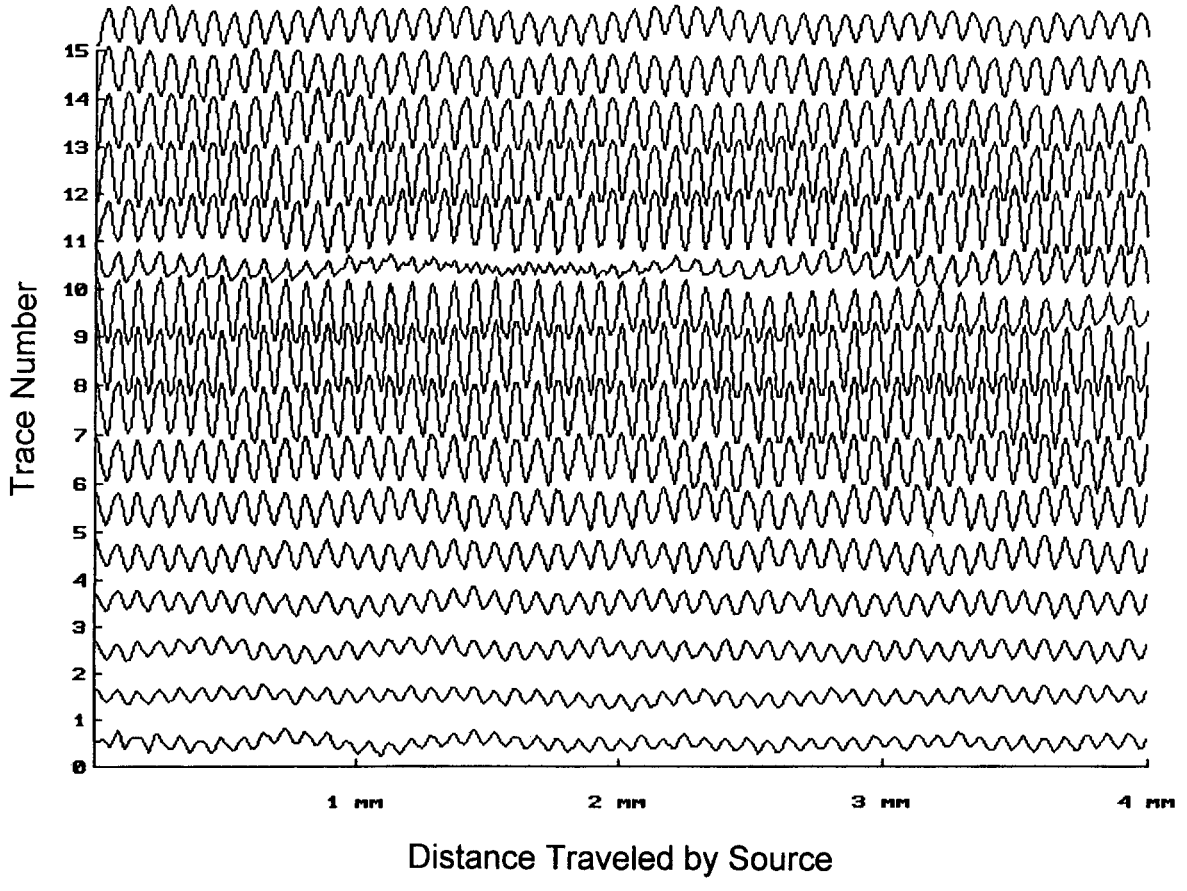

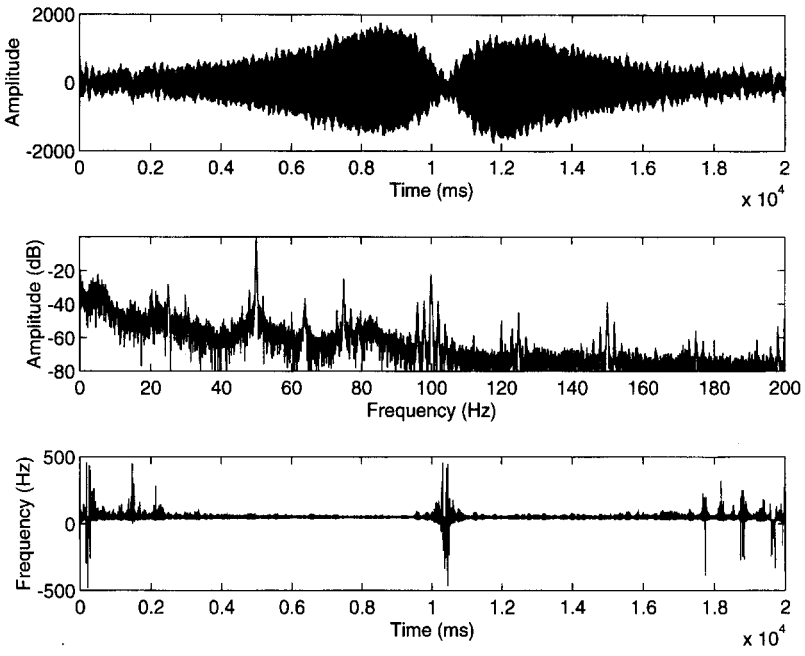

Fig. 4 Compressed time-waveform (*top*), amplitude spectrum (*middle*) and instantaneous frequency (*bottom*) of stimulus shown in Fig. 3

response in the beginning of trace 11 before the response null with that after in the beginning of trace 12 in Fig. 3). As expected, the instantaneous frequency is close to 50 Hz except during times when the stimulus amplitude is low, i.e. when the source is directly opposite the hydrophone and at the beginning and end of source travel, when the source is relatively distant from the hydrophone.

The RMS amplitude of the digitized hydrophone response (symbols) to different source amplitudes is shown in Fig. 5A along with the computer predictions (solid lines) for the pressure distribution based on the flow field equations. The zero crossing point of each function was arbitrarily shifted to X-Position = 61 mm. This is the location at which the source is directly opposite the hydrophone (for stimulus measurement) or the neuromast (for modeled canal results (see Fig. 1)). Plots similar to those in Fig. 5 are shown for varying source distances (Fig. 6A). Plots for varying source heights are not shown, but they are essentially the same as those for source distance due to the bilateral symmetry of the dipole field. Except for a slight elevation of the measured response at low amplitudes near the ambient noise floor, there is good agreement between measured and predicted responses.

The pressure gradient pattern derived from the modeled pressure curves in Figs. 5A and 6A are shown in Figs. 5B and 6B. Each symbol represents the pressure difference between successive pairs of points separated by 2 mm, as illustrated in Fig. 1B. The pressure gradient pictures reveal a complex but predictable pattern consisting of a large, central positive pressure gradient peak surrounded by two, smaller negative peaks on either side. The arrows indicate the source locations where the pressure gradient function passes

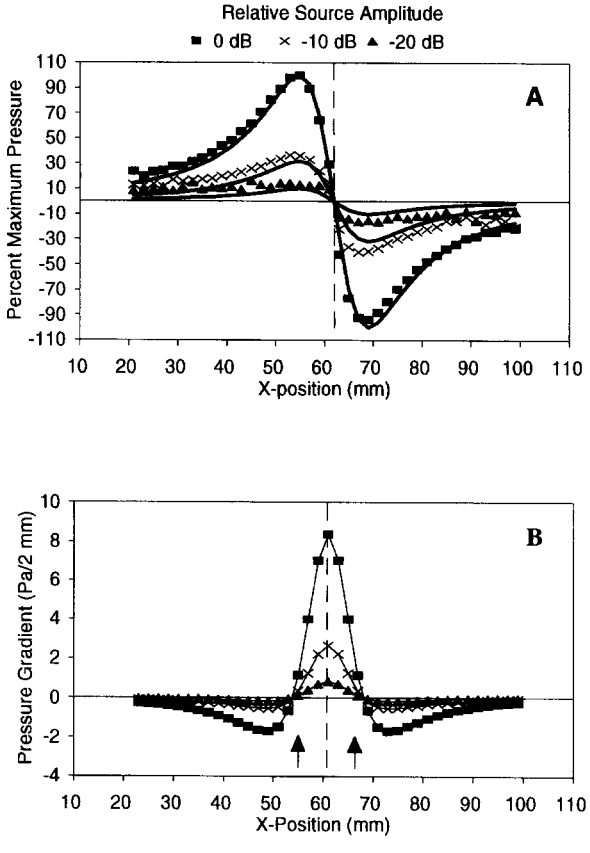

Fig. 5 A Modeled (*solid lines*) vs. measured (*symbols*) pressures in response to changing source locations (*X-positions*) for different relative source amplitudes. Source distance (*Y-axis*) and elevation (*Z-axis position*) were fixed at 10 and 0 mm, respectively. Hydrophone was centered at 61 mm along the x-axis. Positive and negative pressures indicate where responses are 180° out of phase. **B** Pressure-gradient pattern derived from model in **A**. *Arrows* indicate positions of 180° phase reversals and response nulls, which do not change with source amplitude

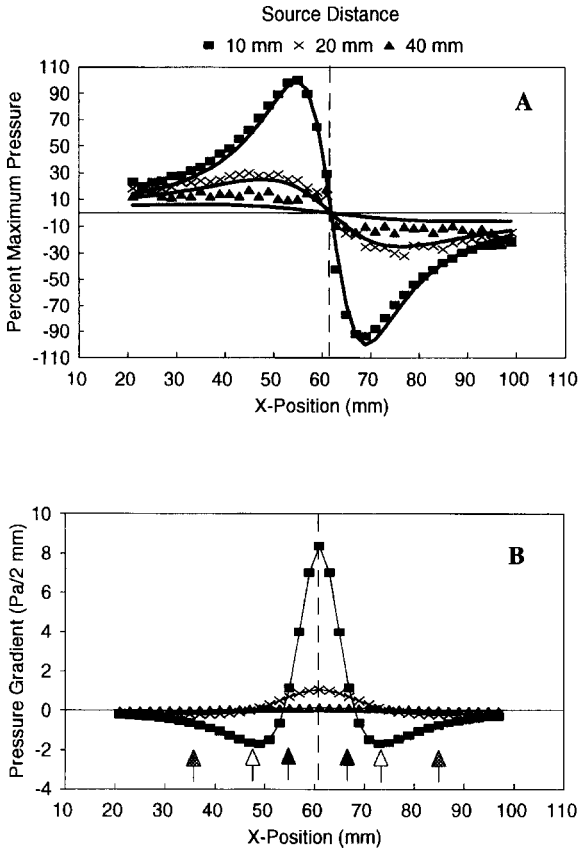

Fig. 6A, B Same as Fig. 5, but for different distances (Y-axis positions). Elevation (Z-axis position) remains constant at 0 mm. Phase reversal and response null positions as indicated by different sets of *arrows* show that the spatial separation between these positions increases as source distance increases

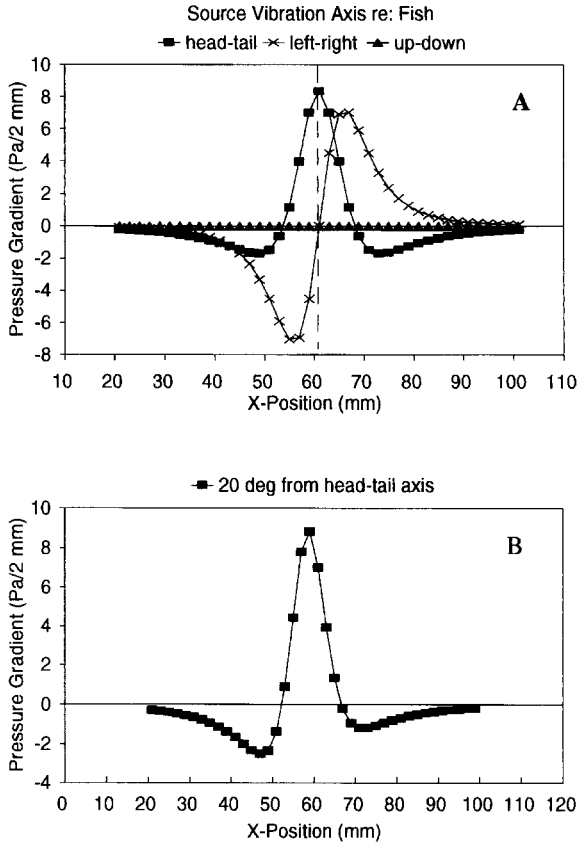

Fig. 7 A Modeled pressure gradient patterns for a head/tail, up/down and left/right axes of oscillation with source distance and elevation fixed as in preceding figures. **B** Modeled pressure gradient pattern across a detector array that is tilted at approximately 20° relative to a head-tail axis of source oscillation

through zero and where the sign of the pressure gradient changes from negative to positive, or vice versa. These are referred to hereafter as the 180° phase-reversal or shift locations. Note that the spatial locations of side peaks and phase-reversals are invariant as a function of source amplitude, but change as a function of source distance (see arrows in Fig. 5B and 6B). As distance increases, the spatial separation between side peaks and phase reversal points increases (Fig. 6B). The peak amplitudes also decrease at the rate of 18 dB/distance doubling, which is equivalent to the 1/distance^3 fall-off rate predicted for dipole sources (Denton and Gray 1983; Kalmijn 1988, 1989).

Figure 7A compares the pressure gradient patterns modeled for three different axes of oscillation relative to the fish: head/tail, left/right, and up/down. In all cases, the patterns were generated for a linear array of detectors (separated by 2 mm) in a single plane through the center of the source (Fig. 1A). The distance between the center of the linear array and source center was 10 mm. The lack of response for the up/down axis reflects the position of the modeled detector array totally within the pressure null area of the dipole field (see Fig. 1A). If the plane of the detector array is moved 10 mm outside of the pressure null area, the resulting pressure gradient pattern (not shown) is a bi-modal pattern like that shown for the left/right oscillation axis (Fig. 7A), except that peak amplitudes are much higher ($\pm$ 90 Pa/2 mm).

As can be seen, the pressure gradient pattern varies with the axis of source oscillation. Whereas a head/tail axis of oscillation produces a tri-modal pressure gradient pattern with two phase-reversal points, left/right and up/down axes of oscillation produce a bi-modal pattern with a single reversal point in the center. Intermediate axes of oscillation (e.g. 20° tilt from head-tail), modeled for cases in which the plane of the detector array does not bisect source center, produce tri-modal patterns with side peak asymmetries (Fig. 7B).

Neurophysiological results

To demonstrate that response patterns of lateral line nerve fibers could be predicted from measured and modeled pressure gradient patterns, we obtained neurophysiological results from 9 posterior lateral line fibers in 5 goldfish. Results are primarily shown for

a single fiber (G11P3) from which we obtained response measures under all control and test conditions for a head-tail oscillation axis – the only oscillation axis used in neurophysiological demonstrations (Figs. 8–11). Because this fiber responded well to frequencies as high as 100 Hz at moderate stimulus amplitudes (normally outside the range of superficial neuromasts, Münz (1989)), we tentatively identified this fiber as a canal neuromast fiber.

Plotted in Fig. 8 are the phase angle (solid circles) and average firing rate (solid squares) responses of fiber G11P3 to different locations of the 50 Hz source along the length of the fish. The source center was at a distance of 10 mm from the lateral surface of the fish and at the same approximate elevation as the trunk canal; oscillation amplitude was approximately at the upper level of the fiber's dynamic range, but just below levels causing saturated responses. Because we observed no systematic differences between spatial event plots determined with tail-head and head-tail directions of movement, results in this and subsequent figures are presented for headward directions only.

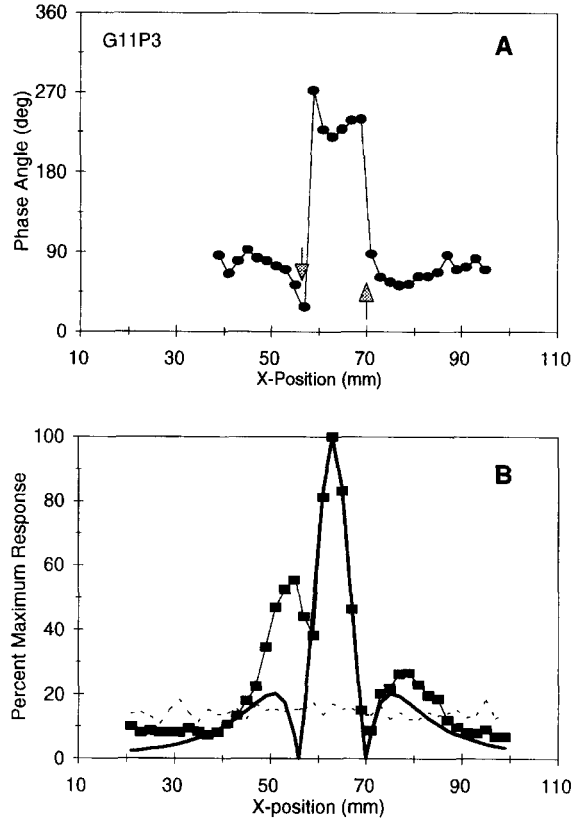

Fig. 8A, B Phase angle (**A**) and average evoked firing rate (**B**) response from fiber G11P3. The evoked rate response (*square symbols*) is compared to rectified pressure gradient predictions (*solid heavy line*) and to spontaneous rates of activity (*dashed line*). Evoked and spontaneous firing rate and pressure gradient predictions have been normalized to percent maximum response. Phase angle measures corresponding to Z values less than 4.6 have been omitted from this figure

When the negative side peaks of the modeled pressure gradient pattern are rectified (heavy solid line, Fig. 8B) for comparison with the neural response pattern, the two patterns are very similar in having a large, central response peak and two smaller side peaks. The rectification of pressure gradient side peaks is needed because the hair cell/afferent fiber response to a sinusoidal signal is essentially rectified. That is, sinusoidal signals cause fluid to move in one direction during one half of the cycle and the opposite direction during the other half. For canal neuromasts, which have two oppositely oriented populations of hair cells (Flock 1965; Best and Gray 1982; Janssen et al. 1987), this means that both populations will cause an increase in the firing rate of afferent fibers during one phase of the cycle, but that the responses from the two will be 180° out of phase with one another. The shift between negative and positive peaks in the pressure gradient stimulus will thus be reflected in the phase angle response of the fiber. The arrows in Fig. 8A point to the locations where the phase angle shifts upward or downward by 180° and where there is a corresponding drop (null) in the firing rate response. As predicted from the pressure gradient pattern, the central response peak is 180° out of phase with the smaller side peaks.

Figure 9 shows what happens to this response pattern when source distance and elevation are kept constant, but source amplitude is varied. As predicted, response nulls and phase-shift locations coincide and do not change with varying source amplitude. In contrast, these locations change systematically when source distance is increased (Fig. 10), as predicted from pressure gradient patterns (Fig. 6). As source distances increases, there is a very orderly increase in the spatial separation between phase reversal locations and between side response peaks.

Note that in Figs. 9–11, we have plotted phase-angles corresponding to Z values less than 4.6 (dashed line in panel C of each figure). We have done this so that entire phase-angle functions can be seen without interruptions and compared with spike rate functions, but note that in many cases, wide fluctuations of phase angle measures correspond to low Z values, indicating that the underlying period histogram distributions are not significantly different from random.

Figure 11 compares the neural response evoked by different locations of the 50 Hz source at a distance of 10 mm to that evoked under three different control conditions: source oscillation in the absence of location changes (source fixed in position at x = 100 mm, y = 10 mm), location changes in the absence of oscillation and the absence of both location changes and oscillation (the latter also plotted as dashed lines in panel A of Figs. 9 and 10). For this fiber, there is a small (10–20 spikes/s) increase in the average firing rate when the source changes location in the absence of sinusoidal oscillations (solid squares). This small response occurs at source locations between 45–75 mm and resembles

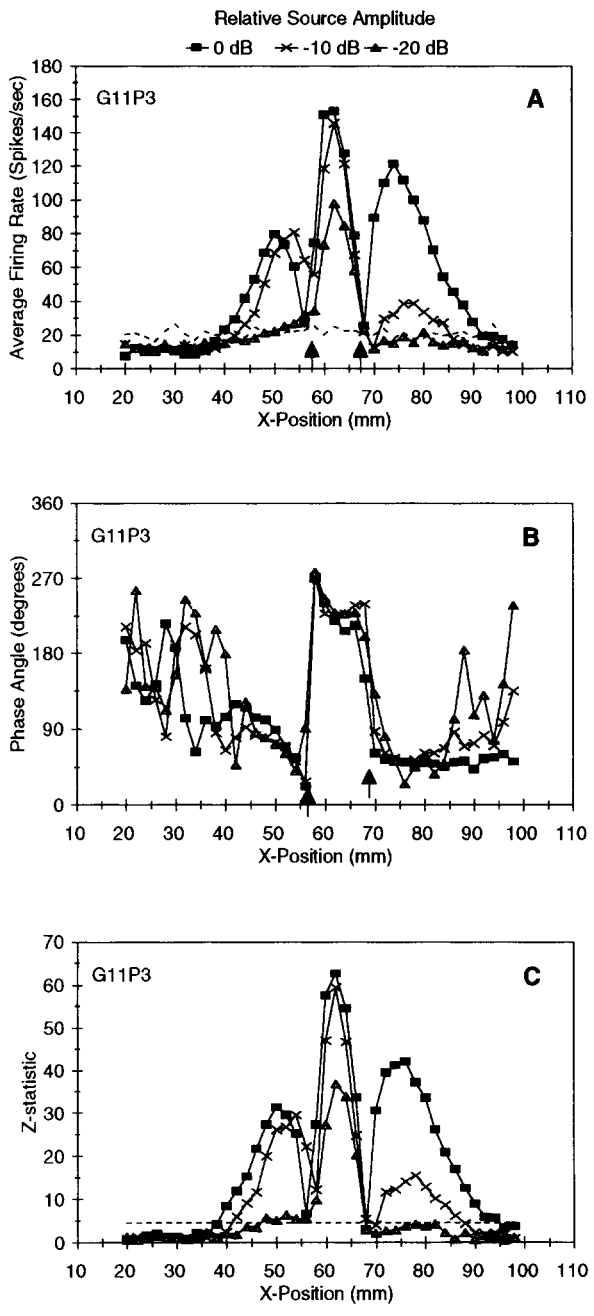

Fig. 9A–C Average firing rate (**A**), phase-angle (**B**) and Z-stat (**C**) measures from a single posterior lateral line fiber responding to the stimulus depicted in Fig. 5. Fish snout was at X-axis position 0, caudal peduncle at position 100. *Arrows* in **A** and **B** indicate positions of response nulls and 180° phase reversal points. *Dashed line* in **A** indicates spontaneous firing rate in the absence of source oscillation and changing source locations. *Dashed line* in **C** indicates a Z-statistic of 4.6 ($P = 0.01$); values below that indicate a possibility that underlying period histogram distributions could be random. Source amplitude is referenced relative to that used when source distance (Fig. 10) was varied

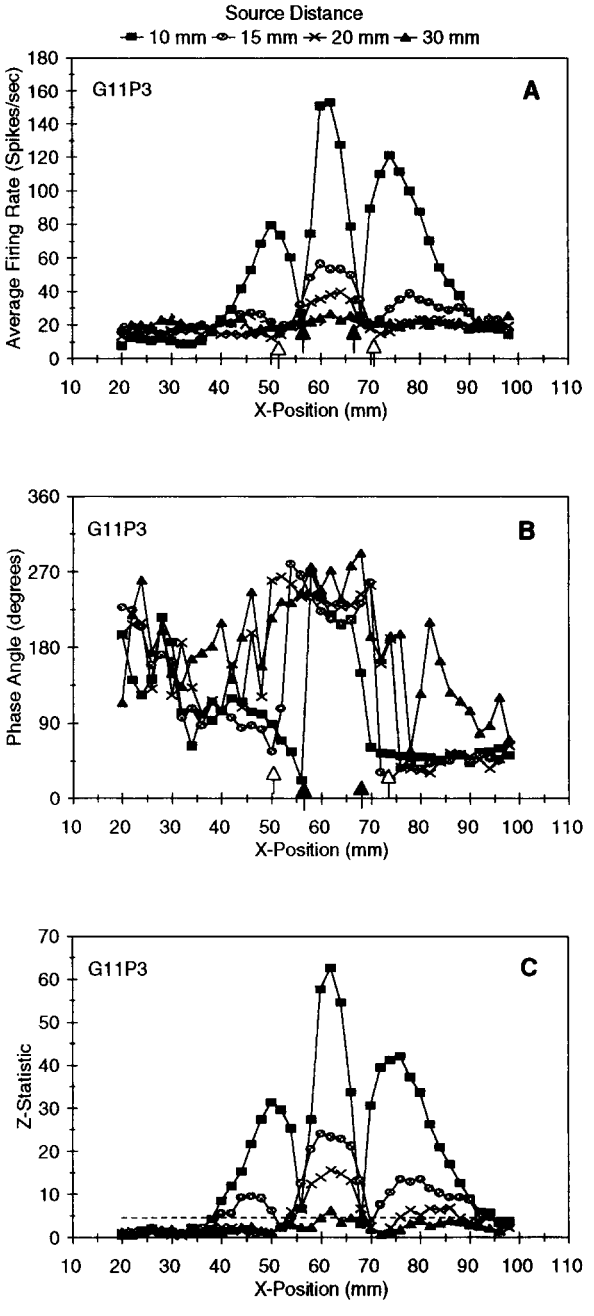

Fig. 10A–C Same as Fig. 9, but for varying source distances as modeled in Fig. 6

the much larger tri-modal response evoked in the presence of 50 Hz sinusoidal oscillation (solid line in Fig. 11). Maximum responses to the oscillating and non-oscillating source occur at approximately the same location (x = 64 mm).

The response in the absence of imposed oscillation may be due to mechanical resonances of the movement-generating system, to the slow linear motion itself (which is also a dipole motion) or to a combination of both. Hydrophone measurements of source movement alone (y = 10 mm) revealed mechanical resonances near 100 Hz that ranged from 15–35 dB down from the lowest and highest 50 Hz source levels used. Although we did not systematically measure the sensitivity of fiber G11P3 to a 100 Hz stimulus, this fiber could be driven by imposed 100 Hz oscillations of the source. Nevertheless, the response of this fiber to movement

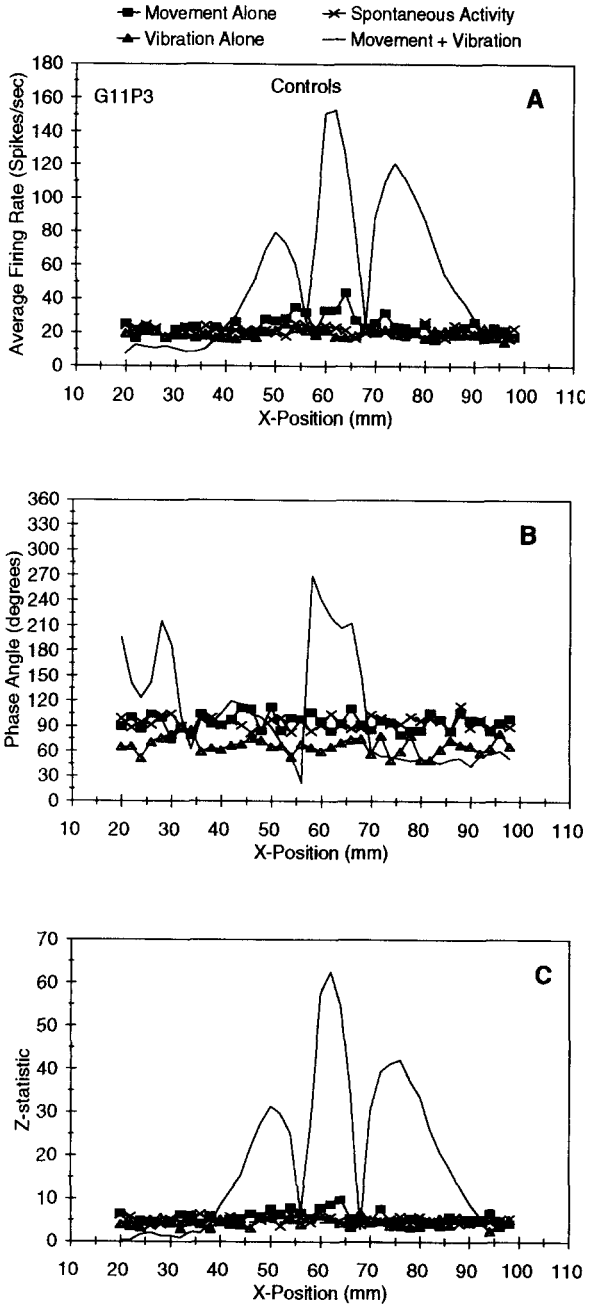

Fig. 11A–C Average firing rate (**A**), phase-angle (**B**) and Z-stat (**C**) measures under various control conditions (*symbols*) and the test condition, in which the source is both oscillating and moving (*solid line without symbols*). Source amplitude = 0 dB, source distance = 10 mm. For the control condition in which the source was oscillated, but not moved, the source was placed at an × position = 100 mm

alone is quite small relative to that evoked by the 50 Hz oscillation + movement and cannot account for the 180° phase shifts (Fig. 11B).

Figure 12 shows the average firing rate response of fiber G11P3 (heavy solid line) along with that of three other fibers for a source 10 to 15 mm away. Note that one fiber had a bi-modal pattern (dashed line) consistent with a pressure gradient pattern created by a source oscillating at 90° relative to the canal (or neuromast) axis. Since the axis of source oscillation was not varied in this study, this fiber most likely innervated a vertically-oriented section of the trunk canal or a superficial neuromast with a dorso-ventral orientation of hair cells. The location of the response center (null) at the caudal edge of the operculum, where the trunk canal is more vertically oriented, and the presence of superficial neuromasts on trunk scales of the goldfish (Puzdrowski 1989), make both hypotheses possible, but the high spontaneous rate of this fiber (60 spikes/s) suggests that it probably innervated a canal neuromast.

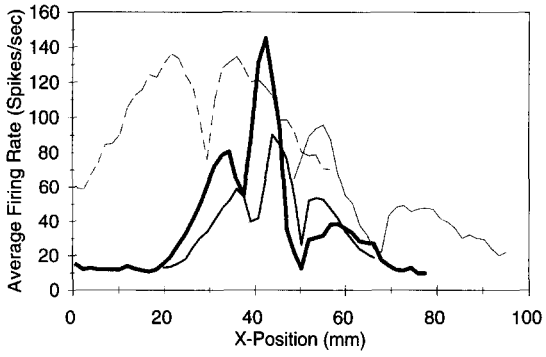

Fig. 12 Average firing rate response patterns from four fibers for a source distance between 10 and 15 mm. Response functions are plotted so that an X-position of 0 mm is at the tip of the fish's snout, 20–30 mm at the approximate edge of operculum, and 100 mm near the base of the caudal peduncle. Note that patterns range from bi-modal (*dashed line function*) to tri-modal (*heavy, medium and thin solid lines*). Note also that range of source motion for all but one fiber (*heavy solid line*, same fiber as in Figs 8–11) was restricted to 50–60 mm. Thus, the assymetrical bi-modal pattern depicted by the thin solid line is probably an incomplete tri-modal pattern

Discussion

These results demonstrate that responses of posterior lateral line nerve fibers to changing dipole locations can largely be predicted from pressure gradient patterns modeled from the dipole field equations (Figs. 8, 9 and 10). For a source that systematically changes its location along the length of the trunk lateral line canal (oscillation axis parallel to the canal), canal neuromast fibers respond with three consecutive response peaks as the source moves past the neuromast. This response pattern can be predicted from the spatial distribution of pressure gradients along the canal modeled for a stationary source (Fig. 1). The pressure gradient stimulus field predicts that the first and third (side) response peaks will be smaller than and 180° out of phase with the second (central) peak and that the central response peak will occur when the source is directly opposite the innervated neuromast.

There are a two ways in which neural response patterns appear to differ from predicted pressure gradient patterns. One is that at high source amplitudes (0 dB) and close distances (10 mm) the ratio between the central and side peak heights are less than predicted (Figs. 9 and 10). This is most likely due to the fact that the fiber is in the saturated range of its rate-level function when responding to source locations associated with the central peak. In fact, when source amplitude is decreased by 10 dB from the maximum level used (Figs. 8 and 9B), the relative heights of central and side peaks are most consistent with the predictions, indicating that the fiber was indeed saturated at 0 dB for the narrow range of source locations evoking maximum responses. Although we have not systematically measured the dynamic ranges of posterior lateral line nerve fibers in the goldfish, those of mottled sculpin fibers are typically 20–30 dB (Coombs and Fay 1993).

Another apparent difference between neural and predicted responses are the asymmetries between headward and tailward side peak responses (Figs. 8, 9 and 10). It is unlikely that these asymmetries are due to the presence of the fish, since Hassan (1993) has shown that the presence of a fish-like model results in an overall increase in velocity amplitudes, but not in the spatial distributions of flow velocity amplitudes. Rather, it is most likely that these asymmetries are due to the fact that the axis of dipole movement and oscillation were not exactly parallel to and centered on the axis of the canal segment containing the innervated neuromast (Fig. 7B). If this interpretation is correct, side peak asymmetries could provide additional information on source orientation and direction of movement.

Although future studies with larger sample sizes and more refined techniques may reveal that these and other slight mismatches between measured and modeled responses are due to biomechanical or neural transformations at the periphery, the current results indicate that a rather faithful representation of pressure gradient patterns by afferent fibers is possible. In light of this faithful representation and the good match between computed and measured pressure gradient patterns, it is also reassuring to note that for small dipole sources at least, long-standing concerns about the near-field 'nightmare' in small tanks and the distortions introduced by tank boundaries and the fish itself need not be paramount. In this context, we would also like to point out that the measurement approach taken here, in which a single miniature hydrophone is used to map the pressure field, can be a very simple and useful approach for predicting the pressure-gradient stimulus to the lateral line.

Because the major purpose of the neurophysiological component of this study was merely to demonstrate that pressure gradient patterns could be encoded by the lateral line periphery, we did not measure response patterns for a large population of goldfish fibers, nor did we systematically explore how patterns of neural response might differ for superficial vs. canal neuromasts or for different neuromast or source orientations. However, bi-modal response patterns obtained from posterior lateral line fibers in both the goldfish (Fig. 12) and the mottled sculpin (S. Coombs and R.A. Conley, 1995, and unpublished) are consistent with responses from neuromasts oriented orthogonally to the oscillation axis. Moreover, Sand (1981) obtained bi-modal response patterns with a single phase reversal in response to vertical (dorso-ventral) source oscillations and tri-modal neural response patterns with two reversals in response to horizontal (rostral-caudal) oscillations from fibers innervating trunk canal neuromasts on the roach, *Rutilus rutilus*. His results are clearly consistent with the pressure gradient predictions made here. Finally, 180° phase reversals surrounded by firing rate peaks due to changing source locations have been observed in primary lateral line afferents in a number of different fish species (Münz 1985; Montgomery et al. 1988; Montgomery and Coombs 1991; Wubbels 1991). Thus, it would appear that encoding of pressure gradient patterns by the lateral line periphery is a fairly common, if not universal, principle.

Bleckmann and Zellick (1993) also recorded responses from primary lateral line afferents to sources moving past another ostariophysan species, *Eigenmannia*, but their study differs from the present one in several respects. First of all, they did not measure the pressure gradient field created by their stimulus, so direct comparisons are difficult to make. Secondly, they did not routinely impose sinusoidal oscillation on their moving source, although as measured in this study, there was very likely some oscillation created by the movement mechanism itself. Thirdly, they varied the velocity of linear motion (from 2.5 to 20 cm/s), which was 1–2 orders of magnitude greater than the single velocity of linear motion used in this study (4 mm/s). Thus, their study was designed to investigate the effects of smooth linear motion, whereas ours was designed to examine the effects of dipole source location.

Despite these differences, there are a number of similarities in the results of the two studies. Given that they saw little or no afferent fiber response at very slow levels of motion (2.5 cm/s), their results are consistent with results from our control experiments showing little or no effects due to slow linear motion in the absence of imposed oscillations. They also observed response patterns with spike rate peaks and valleys. It is conceivable and perhaps even likely that these patterns are caused by the pressure gradient pattern of their moving source, which in theory at least, is a dipole motion. Finally, they showed that for some fibers spike rate peaks were followed by spike rate valleys when the source moved in one direction, but that movement in the opposite direction caused spike rate valleys to be

followed by spike rate peaks. These results are consistent with ours in demonstrating that the locations of response peaks and valleys are independent of movement direction.

Given that pressure gradients can be faithfully encoded by the lateral line periphery, it is perhaps worth noting that for dipole sources, the pressure gradient stimulus fields and thus, the sensory receptive fields are relatively large, complex and dependent on the relative orientations of source and receptor. Thus, previous descriptions of lateral line receptive fields (e.g. Bleckmann and Zellick 1993; Wubbels 1991) should be interpreted with the complexities of the pressure gradient field in mind.

The faithful way in which the lateral line periphery can encode pressure gradient patterns also has important implications for how source location and distance might be encoded, if pressure gradient patterns are preserved in the excitation pattern of spatially-distributed neuromasts and mapped in the CNS. In this study, we modeled the excitation pattern that would exist for a linear array of neuromasts in the trunk canal (Fig. 1). For the case in which the oscillation axis is parallel to the neuromast array, regions of maximum excitation (central response peak of pressure gradient pattern) point to the location of the source. This central region is flanked by two smaller regions of excitation that are 180° out of phase with the central region. Since hair cells are anatomically polarized to respond best to one of two directions along the axis of the canal (Flock 1965a, b), this means that at any given moment in time, fluid in the center of the canal is moving in one direction and exciting one population of hair cells, whereas fluid at the ends of the canal is moving in the opposite direction, stimulating oppositely-oriented hair cells (see also Wubbels 1991).

Despite a clear understanding of the phase encoding capabilities of the lateral line periphery as early as the 1960's (Flock and Wersall 1962; Flock 1965a, b, 1967), the relevance of this ability to the overall function of the lateral line has yet to be fully understood. Furthermore, we know next to nothing about how or if phase information is used in the CNS. The present study indicates that phase information could be important in at least two ways: (1) for inhibitory/excitatory sculpting of receptive fields and (2) for distinguishing between changes in source distance and source amplitude.

Inhibitory/excitatory sculpting of receptive fields is known to exist in nearly every sensory system, including many different octavolateralis systems (for review see Montgomery et al., 1995). In the lateral line system, excitatory/inhibitory interactions are likely to first take place in the medial octavolateralis nucleus (MON), where excitatory inputs from peripheral fibers responding to the central peak of the tri-modal excitation pattern could interact with inhibitory input from fibers responding to the side peaks. The overall effect would be to sharpen the central peak pointing to the location of the source–just as the unrectified pressure gradient pattern suggests (Fig. 1B).

The position of phase transitions in the excitation pattern also contains information about source distance that is not confounded by information used to encode source amplitude. Whereas the size of response peaks decline with decreasing source amplitude (Figs 5 and 9) and increasing source distance (Figs 6 and 10), the phase-reversal locations change only with source distance. As distance increases, the spatial separation between transition points increases. Of course, this kind of information would only be useful for the case in which the axis of oscillation is parallel to the long axis of the canal, because pressure gradient patterns for orthogonal axes of oscillation (e.g. up/down, left/right) result in only one phase transition (Fig. 7A). In these cases, information about source distance is preserved in the spatial separation between response peaks, as would also be the case for tri-modal excitation patterns. Given that lateral line canals have several different orientations on the body of fish, however, it is quite likely that for any orientation of a dipole source, tri-modal response patterns will occur in at least one of the canals and that spatial separations between both phase transitions and response peaks could be used to extract relative source distance.

In these experiments, we have recorded the response of a single fiber innervating one neuromast to different source locations, rather than simultaneously recording responses from multiple fibers from different neuromasts to a fixed source location. Although the latter approach will yield a direct measure of the excitation pattern across a spatial array of neuromasts, we have used the former approach because it is much easier to execute and can predict excitation patterns, assuming that neuromasts are innervated by separate fibers at different locations along the body of the fish.

In the African cichlid fish, *Saratherodon niloticus*, one of the few species where the peripheral innervation pattern has been examined anatomically, it appears that this is the case. Individual trunk canal neuromasts may be innervated by as many as 20 different afferent fibers, but less than 4% of these appear to innervate adjacent canal neuromasts (Münz 1985). Similarly, a row of superficial neuromasts on any given scale were found to be innervated by multiple fibers that branched to innervate all or many of the neuromasts in the same row, but not to innervate rows on different scales. Canal and superficial neuromasts were never shown to be innervated by the same fiber. *Carassius* is similar to *Saratherodon* in that each trunk canal scale contains a single canal neuromast and a row of superficial neuromasts (Puzdrowski 1989). Furthermore, physiological results from the goldfish (present study) and many other species (e.g. Münz 1985; Kroese and Schellart 1987; Coombs and Janssen 1990; Coombs and Montgomery 1992; Montgomery et al. 1994) indicate that

canal neuromast fibers tend to innervate one neuromast only.

This brings us to the important question of whether terminals of peripheral fibers form a somatotopic map in the CNS so that the excitation patterns reported here can be represented centrally. There is considerable evidence to show that there is a crude rostral/caudal map in the MON of different fish species (Claas and Münz 1981; McCormick 1981, 1983; New and Northcutt 1984; Finger and Tong 1984; Blubaum-Gronau and Münz 1987; Derosa and Fine 1988; Puzdrowski 1989; Song and Northcutt 1991; New and Singh 1994). That is, anterior lateral line nerves innervating head neuromasts terminate in a separate part of the nucleus, usually the ventromedial portion of the nucleus, whereas posterior lateral line nerves innervating trunk neuromasts tend to terminate in the dorsolateral portion. The precision of this map remains an open question, however, and a number of investigators using HRP tract tracing techniques have reported considerable overlap in the terminal fields of primary afferents. One interpretation of these results is that there is no precise somatotopic map in the CNS. Given the spatial distribution of lateral line endorgans on the head and body of fish, this would be a somewhat unsatisfying and surprising finding if true.

Another possible interpretation, however, is that somatotopic maps are partially obscured by phase maps, as would be expected if phase mapping were used to provide inhibitory/excitatory sculpting of receptive fields. A distinct separation of fiber terminals in the MON of the skate (Bodznick and Schmidt 1984) and the mottled sculpin (New, personal communication) into two groups suggests a possible substrate for preserving polarity differences at the brainstem level. Furthermore, recent Golgi studies on the MON of the goldfish (New et al. in press) indicate that there are two distinct populations of principal output (crest) cells very similar to basilar and non-basilar pyramidal cells in the gymnotid ELL (Maler 1979). In the gymnotid ELL, excitatory center/inhibitory surround and inhibitory center/excitatory surround receptive fields are attributed to these two classes of cells (Bastian 1986; Maler et al. 1981). Clearly, however, more information on how peripheral polarity differences are mapped in the CNS is needed before any conclusions about its significance for the mechanosensory lateral line system can be reached.

Acknowledgements We would like to thank Joe Bastian for his help and encouragement when these experiments were first being planned and Dick Fay for jump-starting the phase-angle measurements and for providing helpful and insightful comments throughout this work, including the writing of this paper. Thanks are also owed to Dr. John Montgomery for his helpful comments on this work and to David L. Cosnowski for his programming help on the MATLAB software. This work was funded by a NIDCD Program Project Grant and by a grant from the Office of Naval Research.

References

Bastian J (1981a) Electrolocation I. How the electroreceptors of *Apternotnotus albifrons* code for moving objects and other electrical stimuli. J Comp Physiol 144: 465–479

Bastian J (1981b) Electrolocation II. The effects of moving objects and other electrical stimuli on the activities of two categores of posterior lateral line lobe cells in *Apternotus albifrons*. J Comp Physiol 144: 481–494

Batschelet E (1981) Circular statistics in biology. In: Anonymous (ed) Mathematics in Biology. Academic Press, New York, pp 52–83

Bergeijk WA (1964) Directional and nondirectional hearing in fish. In: Tavolga WN (ed) Marine bio-Acoustics. Pergamon Press, Oxford, pp 281–299

Best ACG, Gray JAB (1982) Nerve fiber and receptor counts in the sprat utriculus and lateral line. J Mar Biol Ass UK 62: 201–213

Bleckmann H, Zelick R (1993) The responses of peripheral and central mechanosensory lateral line units of weakly electric fish to moving objects. J Comp Physiol A 172: 115–128

Blubaum-Gronau E, Münz H (1987) Topologische Repräsentation primärer Afferenzen einzener Seitenlinienabschnitte beim Schmetterlingsfisch *Pantodon buchholzi*. Verh Dtsch Zool Ges 80: 268–269

Bodznick D, Schmidt AW (1984) Somatotopy within the medullary electrosensory nucleus of the little skate, *Raja erinacea*. J Comp Neurol 225: 581–590

Claas B, Münz H (1981) Projection of lateral line afferents in a teleost's brain. Neurosci Lett 23: 287–290

Coombs S, Conley RA (1995) Source distance determination by the mottled sculpin lateral line. Fourth International Congress of Neuroethology, Cambridge, England

Coombs S, Fay RR (1993) Source level discrimination by the lateral line system of the mottle sculpin. J Acoust Soc Am 93: 2116–2123

Coombs S, Janssen J (1990) Behavioral and neurophysiological assessment of lateral line sensitivity in the mottled sculpin, *Cottus bairdi*. J Comp Physiol A 167: 557–567

Coombs S, Montgomery JC (1992) Fibers innervating different parts of the lateral line system of the Antarctic fish, *Trematomus bernacchii*, have similar neural responses despite large variations in peripheral morphology. Brain Behav Evol 40: 217–233

Denton EJ, Gray JAB (1983) Mechanical factors in the excitation of clupeid lateral lines. Proc R Soc Lond B218: 1–26

Denton EJ, Gray JAB (1993) Stimulation of the acoustico-lateralis system of clupeid fish by external sources and their own movements. Phil Trans R Soc Lond B 341: 1296, 113–127

DeRosa F, Fine ML (1988) Primary connections of the anterior and posterior lateral line nerves in the oyster toadfish. Brain Behav Evol 31: 312–317

Finger TE, Tong SL (1984) Central organization of eighth nerve and mechanosensory lateral line systems in the brainstem of ictalurid catfish. J Comp Neurol 229: 129–151

Flock Å (1965a) The ultrastructure of the lateral line canal organ. Acta Oto-Laryngol (Suppl) S199: 7–90

Flock Å (1965b) Transducing mechanisms in the lateral line canal organ receptors. Cold Spring Harbor Symp Quant Biol 30: 133–145

Flock Å (1967) Ultrastructure and function in the lateral line organs. In: Cahn PH (ed) Lateral line detectors. Indiana Univ Press, Bloomington, In., pp 163–197

Flock Å, Wersäll J (1962) A study of the orientation of the sensory hairs of the receptor cells in the lateral line organs of fish, with special reference to the function of the receptors. J Cell Biol 15: 19–27

Gray J (1984) Interaction of sound pressure and particle acceleration in the excitation of the lateral-line neuromasts of sprats. Proc R Soc Lond B220: 299–325

Gray JAB, Best ACG (1989) Patterns of excitation of the lateral line of the ruffe. J Mar Biol Ass UK 69: 289–306

Hassan ES (1993) Mathematical description of the stimuli to the lateral line system of fish, derived from a 3-dimensional flow field analysis. III. The case of an oscillating sphere near the fish. Biol Cybern 69: 525–538

Janssen J, Coombs S, Hoekstra D, Platt C (1987) Anatomy and differential growth of the lateral line system of the mottled sculpin *Cottus bairdi* (Scorpaeniformes: Cottidae). Brain Behav Evol 30: 210–229

Kalmijn AJ (1988) Hydrodynamic and acoustic field detection. In: Atema J, Fay RR, Popper AN, Tavolga WN (eds) Sensory biology of aquatic animals. Springer, New York, pp 83–130

Kalmijn AJ (1989) Functional evolution of lateral line and inner-ear sensory systems. In: Coombs S, Görner P, Münz H (eds) The mechanosensory lateral line: neurobiology and evolution. Springer, New York, Berlin, pp 187–215

Kroese ABA, Shellart NAM (1992) Velocity- and acceleration-sensitive units in the trunk lateral line of the trout. J Neurophysiol 68: 2212–2221

Maler L (1979) The posterior lateral line lobe of certain gymnotoid fish: quantitative light microscopy. J Comp Neurol 183: 323–363

Maler L, Sas E, Rogers J (1981) The cytology of the posterior lateral line lobe of high frequency electric fish (Gymnotidae) : Dendritic differentiation and synaptic specificity in a simple cortex. J Comp Neurol 158: 87–141

McCormick CA (1981) Central projections of the lateral line and eighth nerves in the bowfin, *Amia calva*. J Comp Neurol 197: 1–15

McComrick CA (1983) Central connections of the octavolateralis nerves in the pike cichlid, *Crenicichla lepidota*. Brain Res 265: 177–185

Montgomery JC, Coombs S (1992) Physiological characterization of lateral line function in the Antarctic fish (*Trematomus bernacchii*). Brain Behav Evol 40: 209–216

Montgomery JC, Macdonald J A, Housley G D (1988) Lateral line function in an antarctic fish related to the signals produced by planktonic prey. J Comp Physiol A 163: 827–833

Montgomery J, Coombs S, Janssen J (1994) Form and function relationships in lateral line systems: comparative data from six species of antarctic notothenioid fish. Brain Behav Evol 44: 299–306

Montgomery JC, Coombs S, Conley RA, Bodznick D (1995) Hindbrain sensory processing in lateral line, electrosensory and auditory systems: A comparative overview of anatomical and functional similarities. Audit Neurosci 1: 207–231

Morse PM (1948) Vibration and sound. McGraw Hill, New York

Münz H (1985) Single unit activity in the peripheral lateral line system of the cichlid fish *Sarotherodon niloticus* L. J Comp Physiol A 157: 555–568

Münz H (1989) Functional organization of the lateral line periphery. In: Coombs S, Gorner P, Münz H (eds) The mechanosensory lateral line: neurobiology and evolution, Springer, New York, Berlin pp 285–297

New J, Northcutt RG (1984) Central projections of the lateral line nerves in the shovelnose sturgeon. J Comp Neurol 225: 129–140

New JG, Singh S (1994) Central topography of anterior lateral line nerve projections in the channel catfish, *Ictalurus punctatus*. Brain Behav Evol 43: 34–50

New JG, Coombs S, McCormick CA, Oshel PE (1996) Cytoarchitecture of the medial octavolateralis nucleus in the goldfish, *Carassius auratus*. J Comp Neurol (in press)

Puzdrowski RL (1989) Peripheral distribution and central projections of the lateral- line nerves in goldfish, *Carassius auratus*. Brain Behav Evol 34: 110–131

Sand O (1981) The lateral line and sound reception. In: Tavolga WN, Popper AN, Fay RR (eds) Hearing and sound communication in Fishes. New York, Springer, pp 459–478

Song J, Northcutt RG (1991) The primary projections of the lateral-line nerves of the Florida gar, *Lèpisotheus platyrhincus*. Brain Behav Evol 37: 38–63

Wubbels RJ (1991) Phase reversal in the lateral line of the ruff (*Acerina cernua*) as cue for directional sensitivity. Comp Biochem Physiol A 100: 571–573